# We are IntechOpen, the world's leading publisher of Open Access books Built by scientists, for scientists

**4,800**
Open access books available

**122,000**
International authors and editors

**135M**
Downloads

Our authors are among the

**154**
Countries delivered to

**TOP 1%**
most cited scientists

**12.2%**
Contributors from top 500 universities

CLARIVATE ANALYTICS BOOK CITATION INDEX INDEXED

WEB OF SCIENCE™

Selection of our books indexed in the Book Citation Index in Web of Science™ Core Collection (BKCI)

## Interested in publishing with us?
## Contact book.department@intechopen.com

Numbers displayed above are based on latest data collected.
For more information visit www.intechopen.com

16

# Deep Proton Writing: A Rapid Prototyping Tool for Polymer Micro-Optical and Micro-Mechanical Components

Jürgen Van Erps, Michael Vervaeke, Christof Debaes, Heidi Ottevaere, Alex Hermanne and Hugo Thienpont
*Brussels Photonics Team, Dept. of Applied Physics and Photonics, Vrije Universiteit Brussel*
*Belgium*

## 1. Introduction

During the last decades, the use of photonics in data communication and numerous other industrial applications brought plenty of prospects for innovation and opened different unexplored market opportunities. Refractive micro-optical and micro-mechanical structures like 2-D arrays of spherical micro-lenses, micro-prisms and cylindrical micro-lenses or mechanical alignment features such as 2-D fiber array holders, are likely to be combined with optoelectronic devices and optical fibers to play a key role in optical interconnection technology, in massive parallel optical sensors or in high-definition display and projection systems. This vast domain of applications is a major driving force for the fabrication of these micro-optical and micro-mechanical structures (MOMS) and their accurate alignment and integration into opto-mechanical modules and systems. Technologies that enable the fabrication of monolithic, robust and replicable modules which integrate these individual micro-opto-mechanical components are scarce however. Indeed, the rapid prototyping of micro-optical structures is a highly challenging task since the surfaces of the resulting structures should have a sufficient optical quality. This means that the surface flatness should be controlled within a sub-micrometer scale and that the resulting surface roughness should be only a fraction of the operating wavelength (e.g. $\lambda/20$).
By far the most conventional fabrication method that can obtain the required resolution is photolithography, which transfers very fine two-dimensional patterns from a mask into a thin layer of photosensitive material. However, this technique is limited to the patterning of flat surfaces (e.g. to create layers for different transistor parts in micro-electronic circuits). Nevertheless, it is often desirable to create more extensive 3D structures to fabricate micro-optical systems, integrated micro-sensors, micro-fluidic systems or medical devices. Therefore, new technologies are being developed, which enable the micro-structuring of deep geometries. A first technology is laser photoablation, a method in which a sample is exposed to such intense light pulses that some of the material at the surface is being spontaneously evaporated (Mihailov & Lazare, 1993). A second one is the LIGA (German acronym for Lithografie, Galvanoformung und Abformung) technology, in which a polymer substrate is

exposed to a collimated beam of high-energy X-rays, penetrating deep into the substrate with negligible diffraction (Becker et al., 1986). Stereolithography is a novel approach to solidify selected regions from liquid photopolymers layer by layer using a scanning laser (Zhang et al., 1999). In addition, there exist a series of soft-lithograhic techniques (Acharya et al., 2003; Love et al., 2001) to replicate patterns made with conventional lithography, via molding or stamping or by direct printing. These techniques can be applied to a range of substrates which can even can be highly curved (Rogers, 2001) to form 3D structures. A final method capable of fabricating high-precision elements is diamond machining (Davies et al., 2003; McClure, 1991), a mechanical machining process using diamond-tipped cutting elements. It is a multi-stage process which can achieve a nanometer level surface finish and sub-micrometer form accuracies. However, this technique produces a relatively high percentage of defective parts, leading to a high manufacturing cost.

We introduce deep proton writing (DPW) as a candidate technology for the rapid prototyping of a wide variety of micro-optical, micro-mechanical and micro-fluidic components with plenty of applications in photonics (Debaes et al., 2005; Thienpont et al., 2001). Its concept is somewhat comparable to LIGA X-ray lithography (Ehrfeld & Schmidt, 1998), but it uses ions rather than electromagnetic radiation to structure the resist sample. The strength of the DPW technology is its ability to fabricate monolithic building blocks that include micro-optical and micro-mechanical features which allow precise integration in more complex photonic systems. Furthermore, DPW is compatible with low-cost mass-replication techniques. Indeed, once the master component has been prototyped, a metal mould can be generated from the DPW master by applying electroplating. After removal of the plastic master, this metal mould can be used as a shim in a final micro-injection moulding or hot embossing step.

In this chapter, we will give an overview of the process steps of the technology and the characteristic qualities we can expect from the components made by DPW. More in particular, we will describe the ion interactions, the irradiation process, the etching process to create optical surfaces and the swelling process which uses in-diffusion of monomers to create micro-lenses. The general overview of the technology is followed by several examples of different micro-optical components that were fabricated using DPW, targeting applications in optical interconnections and in bio-photonics.

## 2. Deep proton writing

DPW is a generic technology for the rapid prototyping of a wide variety of micro-optical and micro-mechanical components (Debaes et al., 2006). Its concept finds its origin in the LIGA-technology but differs on two important aspects. First, it is based on the use of protons rather than electromagnetic X-ray irradiation to pattern polymer samples. Second, the DPW technology is using a direct writing methodology as opposed to the projection lithography which is being adopted in the LIGA-process, where expensive masks are required for each new LIGA design. In fact, the thick masks required in the LIGA technology are made in steps, by repeating the LIGA process with a gradually higher energy until a mask with a sufficient thickness can be electroplated. Both differences make that the DPW process requires less infrastructural demands and has the potential of being a more flexible technology for rapid prototyping. The deep proton writing process is based on the fact that irradiating swift protons onto a poly(methyl methacrylate) (PMMA) sample featuring linear polymer chains (i.e. the opposite of cross-linked) of high molecular weight, will rupture the long chains

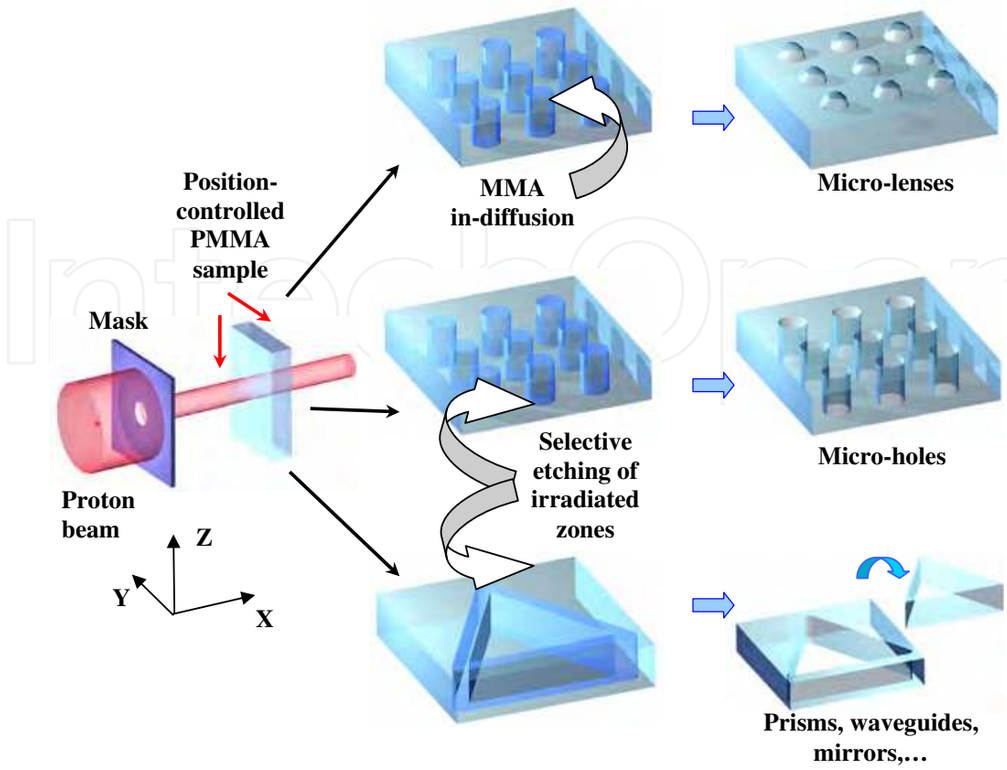


Fig. 1. Deep Proton Writing: basic processing steps. After a patterned irradiation we can either apply a binary chemical etching to remove the irradiated regions or we can in-diffuse a monomer vapor to create micro-lenses through a swelling process. Both processes can be applied to the same sample.

and free radicals will be created in the polymer. As a consequence, the molar mass of the irradiated material will be reduced, resulting in material properties that are very different from those of unexposed bulk material. Two different chemical steps were developed that can be applied to the proton-bombarded areas. The first consists of etching the exposed areas with a specific developer to produce micro-holes, micro-mirrors and micro-mechanical structures. This allows for the fabrication of (2-D arrays of) micro-holes, optically flat micro-mirrors and micro-prisms (with a typical surface roughness well below 20-$nm$ over an area of 48-$\mu m$ x 60-$\mu m$), as well as alignment features and mechanical support structures. The second process involves the in-diffusion of an MMA monomer to locally swell the irradiated zones. This will result in micro-spherical or micro-cylindrical lens surfaces (Ottevaere et al., 2006). Both processes can be applied to the same sample after a single irradiation session as the dose required for etching or swelling is very different. The basic process steps of DPW are illustrated in Fig. 1.

While DPW is clearly not a mass fabrication technique as such, one of its assets is that once the master component has been prototyped, a mould can be generated from the DPW master, which can then be used as a shim in a final replication step. Our in-house technology of elastomeric moulding and vacuum casting (Desmet et al., 2007) allows for the formation of a silicone mould without destruction of the DPW master, but this mould has a limited lifetime of about 10-20 replicas, and the cycle time of the vacuum casting replication is also very

long (Van Erps et al., 2008). On the other hand, a metal mould can be generated from the DPW master by applying electroplating (Wissmann et al., 2008). This metal mould can then be used in a final micro-injection moulding or hot embossing step (Heckele & Schomburg, 2004). This way, the master component can be really mass-produced at low cost in a wide variety of high-tech plastics (Van Erps et al., 2008a).

### 2.1 Ion interactions

The kernel process of DPW is the exposure of selected regions of the sample to accelerated protons. In comparison to photolithographic techniques where the exposure is governed by electromagnetic radiation, the energy transfer of protons with the target material is fundamentally different. In UV lithography, the absorption of the beam is governed by the well-known Lambert-Beer law which states that the fractional absorption is constant along the penetration axis. This results in an exponential decay of absorbed light quanta along their path. In X-ray lithography, the energy that is released when a photon is absorbed, is higher than the binding energy. Hence, such an event can create, apart from inner shell transition, secondary free electrons through the photoelectric effect. These electrons with high kinetic energy are capable of locally breaking the long polymer chains of the target material.

In contrast, the charged particles in an ion irradiation (more specifically a proton irradiation) will only travel to a certain depth in the target, depending on their energy. Indeed, as the ions penetrate the target, they gradually transfer energy to the host material mostly by interaction with the bonded electrons of the target. This electric stopping power and associated range of ions in solids has been a domain of vivid research since the discovery of energetic particle emission from radioactive materials. In 1913 Bohr established a model based on classical mechanics to describe the stopping of ions in matter (Bohr, 1913). This was later refined to a quantum mechanical approach in 1930 by Bethe and Bloch (Bethe, 1930). Since then various scientists have contributed to the subject. Extensive reviews can be found in (Bohr, 1948; Fano, 1963; Kumakhov & Komarov, 1981; Ziegler, 1980).

It turns out that the stopping power (defined as the energy transfer per unit of penetration depth, $dE/dx$) is small at the early part of the ion trajectory. This energy transfer will gradually slow down the swift ions while their interaction density with the PMMA molecules increases. This will result in a maximum energy transfer (and hence absorbed dose) when the impinging ions have a velocity equal to that of the electrons in the amorphous host material. Below this energy level, the energy transfer will abruptly decrease and after a further penetration of a few micrometers, the ions will come to a complete stop. The absorbed dose profile for a proton irradiation of PMMA can be found in Fig. 2. We can see that if we are using protons with an energy of 8.3-$MeV$, their penetration range in PMMA is about 750-$\mu m$. Since our standard PMMA substrate thickness is 500-$\mu m$, this means that the protons will completely traverse the target. Along their penetration path, the protons will cause electron excitation and ionization of the molecular chains and hence induce stresses inside the molecular chains (Lee et al., 1999). These stresses lead to scissions of the polymer chains, resulting in a local degradation of the irradiated PMMA samples. Since the irradiated zones have other physical and chemical properties than the bulk material, it possible to subsequently perform a selective chemical etching or swelling step. The reduced molar mass or molecular weight $M_{irr}$ after the absorption of a dose $D$ (in $J/kg$) can be expressed as a function of the

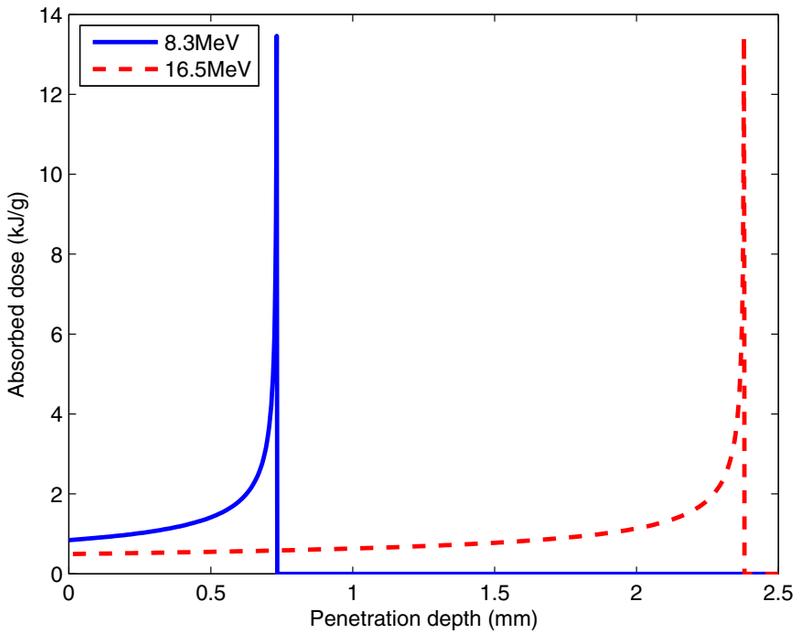


Fig. 2. 1D absorbed dose profile in PMMA after irradiation with a proton fluence of $1.2 \times 10^6 / \mu m^2$ for two different entrance energies (8.3-$MeV$ and 16.5-$MeV$).

initial molecular weight $M_0 = 10^6 g/mol$:

$$\frac{1}{M_{irr}} = \frac{1}{M_0} + \frac{GD}{100eN_A} \tag{1}$$

where $e$ is the elementary charge and $N_A$ is Avogadro's number. The factor $G$ is the yield for main chain scissions per absorbed energy of 100-$eV$. Detailed studies of the molecular mass before and after the irradiation step by means of gel permeation chromatography and micro-thermal analysis confirmed that the chain scission yield $G$ is equal to one (Volckaerts, 2004). The deposited dose $D$ is related to the incoming proton fluence $F$, i.e. the number of impinging protons per unit surface, and the stopping power $dE/dx$ of the swift protons in PMMA, and is given by:

$$D = \frac{F}{\rho_{PMMA}} \frac{dE}{dx} \tag{2}$$

where $\rho_{PMMA}$ is the mass density of the PMMA sample (1.19-$g/cm^3$).
Besides the gradual energy transfer from the protons to the PMMA target material, some spatial straggling of the impinging protons will occur while they are penetrating into the PMMA. In contrast to energy transfer, these straggling effects are primarily governed by multiple ion-ion (nuclear) interactions (Volckaerts, 2004). This straggling will result in a dose deposition slightly outside the targeted volume of the PMMA substrate and will slightly decrease the steepness (i.e. the flatness along the penetration axis) of the optical surfaces of the fabricated micro-structures after the etching process. We have developed an algorithm which can predict the dose profile after a proton irradiation that includes both stopping power and ion-ion scattering effects. In Fig. 3, we plot the resulting 2D absorbed dose profiles for a proton

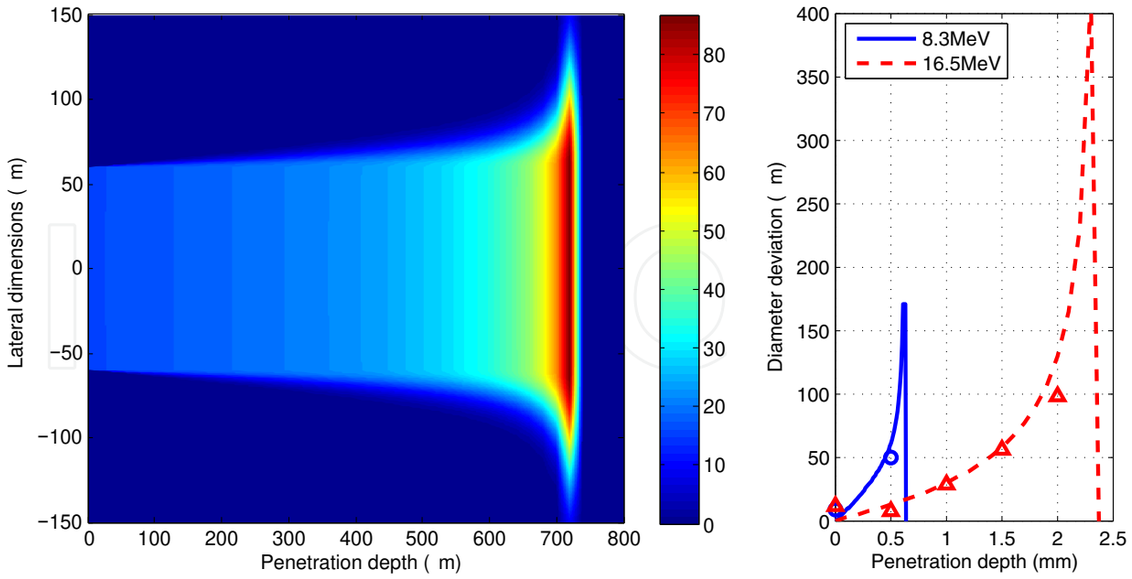


Fig. 3. Left: 2D absorbed dose (in kJ/g) for an irradiation in PMMA with a proton fluence of $1.9 \times 10^7 / \mu m^2$ for an entrance energy of 8.3-$MeV$. Right: Simulated versus experimentally measured increase in hole diameter vs. penetration depth for 8.3-$MeV$ and 16.5-$MeV$ protons.

irradiation in PMMA through a 100-$\mu m$ aperture for two different proton energies (8.3-$MeV$ and 16.5-$MeV$). We can see that within the first 500-$\mu m$, the dose widening due to straggling is a few microns for protons with 8.3-$MeV$ entrance energy. Recently, we have started to use proton beams of 16.5-$MeV$ to reduce the straggling effect even further, as can be observed from the right part of Fig. 3. This 16.5-$MeV$ entrance energy allows us to pattern PMMA samples up to 2-$mm$ thick, resulting in extremely deep structures with high aspect ratio.
Conventionally we would like to keep this straggling effect as small as possible to create deep optical surfaces with high aspect-ratio. However, in some cases we can use the straggling effect to our benefit. This is the case when fabricating conically shaped fiber connector holes to ease the fiber insertion. This will be explained more in detail in section 3.1.

### 2.2 The irradiation process

For our deep proton writing process, we use the CGR-MeV Model 560 Cyclotron facility of the Vrije Universiteit Brussel to fabricate micro-optical and micro-mechanical components. This cyclotron is capable of producing quasi-monoenergetic ($\Delta E/E = 1\%$) proton beams in the energy range between 3-$MeV$ and 45-$MeV$. The accelerated protons are transferred to our DPW irradiation chamber via a set of focusing quadrupole magnetic lenses and switching magnets. The DPW irradiation setup is depicted in Fig. 4. In this figure the protons enter the irradiation vacuum chamber from the left-hand side.
In order to avoid beam scattering and energy loss of the protons along their trajectory, we perform all the irradiations under vacuum conditions (with a pressure below $10^{-4} mbar$). Depending on the settings of the focusing magnet coils, the proton beam will enter the setup with a divergence of a few milliradians. A scintillator that can be inserted into the proton beam allows us to perform beam monitoring to check its shape and uniformity. Then, a set of collimators reduces the beam to a pencil-like uniform beam with the desired diameter. A

first water-cooled aluminium collimator reduces the diameter of the entering beam from a few centimeters to a few millimeters. A second collimator reduces the beam size further to about 2-$mm$. Then, there is a mechanical shutter driven by a small electromotor which can block the beam within a 1-$ms$ timespan.
The final mask element is either a 300-$\mu m$ thick Nickel stopping plate or a stack of two 350-$\mu m$ thick Nickel plates (each fabricated by means of the LIGA technology). The stacking of the Nickel plates is done through high-accuracy metal guide pins with a diameter of 700-$\mu m$. The first mask contains different circular apertures with diameters ranging from 1-$mm$ down to 20-$\mu m$, whereas the second mask contains various apertures of different sizes, but also with different geometries (circular, square, rectangular, elliptical and hexanogal apertures). By changing the position of the stopping mask we can select the desired final proton beam sizes (and shape) on-the-fly during an irradiation. The 300-$\mu m$ mask is capable of stopping 8.3-$MeV$ proton beams, whereas the stack of the two 350-$\mu m$ plates can stop a proton beam of 16.5-$MeV$.

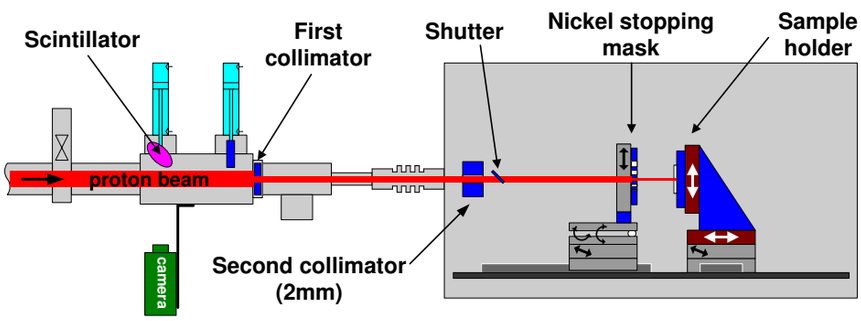


Fig. 4. Schematic overview of the DPW irradiation setup.

The PMMA sample is positioned in a metal holder which is mounted on a biaxial translation stage with a 50-$nm$ accuracy over a total travel range of 25.4-$mm$. Because the initial proton energy is chosen high enough as such that the protons completely traverse the PMMA samples, they induce a charge in a measurement probe located directly behind the target. This allows us to monitor the proton current and the total amount of particles hitting the sample by integrating the proton current during the irradiation, which in turn allows the setup to compensate for fluctuations in the proton current of the cyclotron (Vynck et al., 2002). The dose measurement is based on a precision-switched integrator trans-impedance amplifier. It provides us with a measurement resolution better than $250 \times 10^{-15} C$, which is two orders of magnitude smaller than the minimum proton charge required for our purposes. For a point irradiation, the relation between the collected charge $Q$ and the proton fluence $F$ can be expressed as:

$$Q = eF\frac{\pi d^2}{4} \tag{3}$$

where $d$ is the aperture diameter.
Since PMMA is a positive resist, the irradiated areas can be developed in a subsequent chemical etching step. This means that we have to irradiate the entire contour of the designed component. To create this contour, the PMMA sample is quasi-continuously translated in steps $\Delta x$ of 0.5-$\mu m$ perpendicularly to the beam. At each step, the collected proton charge is measured, and when this value reaches the required proton charge, the microcontroller

system will move the sample to the next position, one step away. The dose profile after a line irradiation will not be completely uniform as it will be an overlap of different circular point irradiations. The peak proton fluence $F_{max}$ in this case will be given by:

$$F_{max} = \frac{4Q_{step}}{e\pi d\Delta x} \tag{4}$$

### 2.3 The etching process

As a next step, a selective etching solvent can be used for the development of the irradiated regions. This allows for the fabrication of (2D arrays of) micro-holes, optically flat micro-mirrors and micro-prisms with high optical quality, as well as alignment features and mechanical support structures.

For the wet etching process, we make use of so-called GG developer (consisting of 60% diethylene glycol monobutyl ether, 20% morpholine, 5% 2-aminoethanol, and 15% de-ionized (DI) water) as the etching solvent. For standard components (in 500-$\mu m$ thick PMMA), etching lasts 1 hour at a temperature of 38°C. During the whole process, the etching mixture is stirred by an ultrasonic stirrer. The etching is stopped by dipping the component in a stopping bath consisting of 20% DI water and 80% diethylene glycol monobutyl ether during 5 minutes. Finally the component is rinsed in DI water.

The dissolution or etching rate can be expressed as (Papanu et al., 1989):

$$v_{etch} = \frac{c_0}{(M_{irr})^n} exp\left(\frac{-E_a}{kT}\right) \tag{5}$$

where $c_0$, $n$ and the activation energy $E_a$ are system-dependent parameters. Combining the above equation with equations (1) and (2), we get the following relation between the proton fluence and the etching rate:

$$v_{etch} = c_0 \left(\frac{1}{M_0} + \frac{G\frac{F}{\rho_{PMMA}}\frac{dE}{dx}}{100eN_a}\right)^{-n} exp\left(\frac{-E_a}{kT}\right) \tag{6}$$

Fitting the above relation to experimentally obtained etching rates of irradiated zones, results in the following values: $c_0 = 2.78 \times 10^{26}$, $E_a = 1.05\text{-}eV$ and $n = 2.9$.

To get an insight into the limits of the flatness of the created surfaces, we need to make a distinction between the direction along and the direction perpendicular to the proton trajectory. Along the proton trajectory the most important parameters that are affecting the surface flatness are the divergence of the incoming proton beam and the straggling of protons along their path by multiple ion interactions as described in section 2.1. The flatness of surfaces in the direction perpendicular to the beam is limited by the precision of the movement of the translation stages (which have a closed loop accuracy of 50-$nm$). The roughness of the obtained surfaces is mainly determined by accuracy of the proton fluence measurement and the beam pointing stability.

We have recently optimized the surface quality of the etched surface after an 8.3-$MeV$ irradiation with our smallest mask aperture of 20-$\mu m$. With this proton beam size, an error in the postion of the beam will be more pronounced and the signal-to-noise ratio of the measured proton current will be significantly smaller than with our standard 140-$\mu m$ proton beam (as the proton current is 49 times smaller to obtain an equal proton fluence). Nevertheless, we succeeded in creating very high quality surface profiles even with this

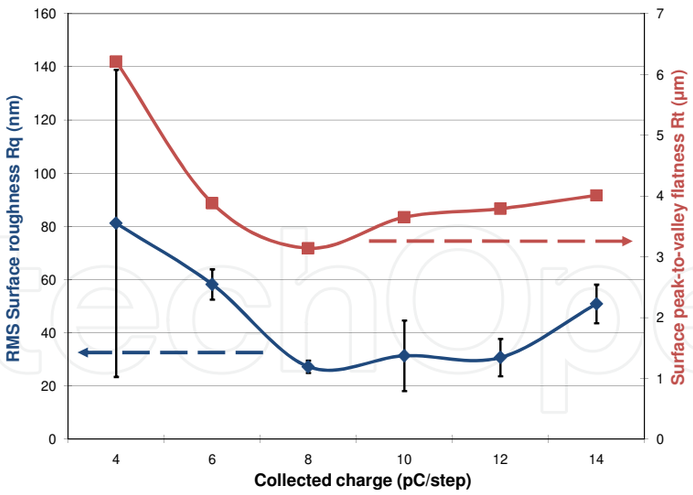


Fig. 5. Surface roughness $R_q$ and flatness $R_t$ as a function of the deposited charge in each 0.5-$\mu m$ step when using a 20-$\mu m$ aperture.

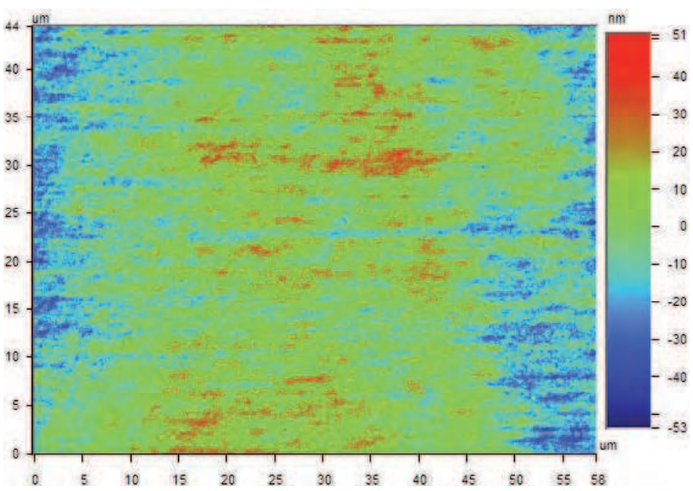


Fig. 6. 2D profile of a DPW-fabricated optical surface, resulting in a typical RMS surface roughness $R_q$ of 18.6-$nm$ for a charge collection of $8 \times 10^{-12} C$ per step of 0.5-$\mu m$.

aperture (Van Erps et al., 2006). In Fig. 5, the resulting local surface root mean square (RMS) roughness ($R_q$) and peak-to-valley flatness ($R_t$) are given as a function of the deposited proton charge per step. $R_t$ was measured over a length of 500-$\mu m$ along the proton trajectory and $R_q$ was calculated by averaging several measurements on an area of 44-$\mu m \times$ 58-$\mu m$ with a non-contact optical surface profiler (WYKO NT2000, Veeco). From this graph, we can conclude that the best results are obtained when we irradiate the sample with a collected proton charge of $8 \times 10^{-12} C$ per step of 0.5-$\mu m$ corresponding to a peak proton fluence of $6.4 \times 10^6 / \mu m^2$. Fig. 6 shows a typical surface profile of a DPW-fabricated optical surfaces. It shows an RMS surface roughness $R_q$ of 18.6-$nm$. Fig. 7 shows the surface profile in the direction of the proton trajectory with a surface flatness $R_t$ of 2.44-$\mu m$. These results are on

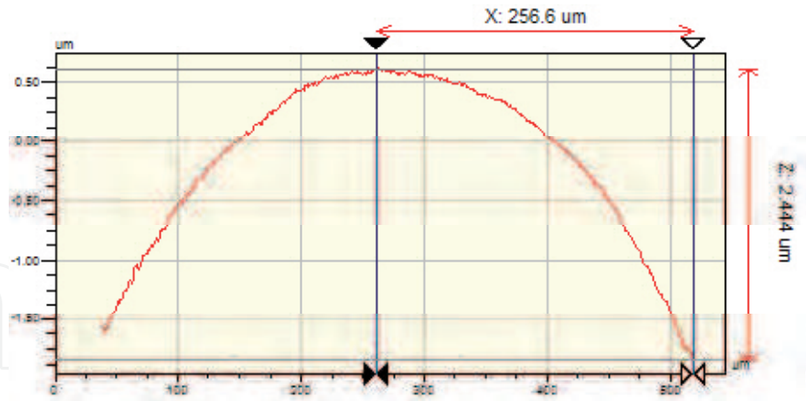


Fig. 7. Surface profile along the proton penetration path, resulting in a peak-to-valley flatness $R_t$ of 2.44-$\mu m$ for a charge collection of $8 \times 10^{-12} C$ per step of 0.5-$\mu m$.

par with the surface roughness and the flatness results we are obtaining with larger mask apertures at the same entrance energy of 8.3-$MeV$.

### 2.4 The swelling process

The swelling process step will create hemispherical surfaces of the irradiated zones which received a dose that was programmed to be too low for the preceding etching step. By exposing the sample to a controlled organic methyl methacrylate (MMA) vapor environment at a temperature of 70°C, the irradiated regions with a sufficiently low molecular weight will be receptive to an in-diffusion of the organic monomer upon which their volume will expand. This way, irradiated regions with a circular footprint will be transformed into hemispherically shaped micro-lenses (Ottevaere et al., 2002).

To swell the micro-lenses we are currently using a diffusion reactor at 70°C. After stabilization of the temperature (within 0.2°C), the MMA monomer is injected into the chamber such that it creates a saturated MMA vapor. The monomer vapor will now diffuse into the irradiated zones to create hemispherically shaped micro-lenses. After 40 minutes, the volumetrically expanded are stabilized by UV-illumination during 1 hour while keeping the temperature at 70°C. For more details on the physics behind the technological processing steps, we refer to (Ottevaere et al., 2002). We demonstrated that DPW is a flexible technology to fabricate 2D matrices of spherical micro-lenses with different diameters between 120-$\mu m$ and 200-$\mu m$ and focal numbers ranging from 1 to 7 on the same PMMA substrate.

We use an optical non-contact surface profiler to measure the geometrical characteristics of the micro-lenses such as lens sag (i.e. height with respect to the substrate) and lens diameter. For the optical characteristics we use a Mach-Zehnder interferometer constructed at the Erlangen Nürnberg University to measure the wave aberrations such as the Point Spread Function (PSF), the Strehl ratio and the Modulation Transfer Function (MTF). In Fig. 8 a plane wave Mach-Zehnder interferogram is given of an array of DPW-fabricated spherical micro-lenses with a different lens sag (increasing from left to right). A detailed comparative study between the obtained DPW micro-lenses and several other fabrication technologies was performed (Ottevaere et al., 2006). In Fig. 8b we show the measured wave-aberration of a typical DPW micro-lens with a high focal number ($f_{\#} = 5.35$). The measured wave aberrations of this micro-lens have an RMS value of $\lambda/5$ which is above the Maréchal criterion

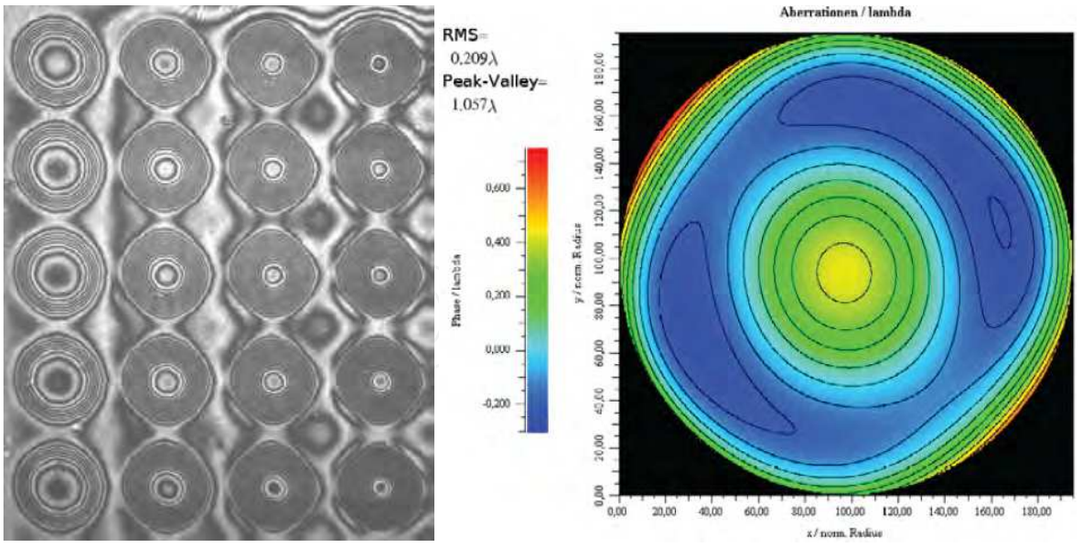


Fig. 8. Left: Plane Wave Mach-Zehnder transmission interferogram of spherical micro-lenses with various lens sags. Right: Contour plot of the wave aberations (RMS value of 0.209$\lambda$, Peak-to-valley of 1.057$\lambda$, distance between lines 0.1$\lambda$) for a 200-$\mu m$ diameter lens with sag of 9.77-$\mu m$

to obtain diffraction limited lenses ($\phi_{RMS} \leq \lambda/14$). We can conclude that although fabrication techniques exist that yield higher quality micro-lenses, the advantage of the DPW approach is that the lenses can be relatively rapidly prototyped and can be monolithically integrated into complex micro-systems (since the swelling process can be combined with the etching process on a single sample).
Within large arrays of DPW micro-lenses, we typically obtain an excellent lens sag uniformity of 0.3%. However, when the micro-lenses are brought in close proximity we need to account for a small and deterministic change in the lens sag. This can be easily compensated for by giving the peripheral lenses of the array a slightly lower dose during the irradiation step. For example, when micro-lenses with a diameter of 140-$\mu m$ are created on an array with a 250-$\mu m$ pitch, the peripheral lenses need a 3% lower dose to obtain the same lens sags over the whole array. Our sample-to-sample repeatability is however much lower. Therefore, efforts have been made to perform an in-situ monitoring of the lens swelling behaviour during the swelling process (Gomez et al., 2008). This allows us to stop the swelling process (and initiate the UV stabilization) when the desired lens height has been achieved.

## 3. Micro-components targeting optical interconnect applications

In this section, we give an overview of the DPW components that were fabricated in recent years with an application in the field op optical interconnects. Our research in this field aims at overcoming the remaining hurdles to massively introduce photonic interconnects in digital systems, as illustrated in Fig. 9. The components we have fabricated to this end include: high-precision two-dimensional single-mode fiber connectors, out-of-plane coupling structures featuring high-quality 45° and curved micro-mirrors for printed circuit board-level interconnections, arrays of high aspect ratio micro-pillars, and free-space intra-chip optical interconnection modules.

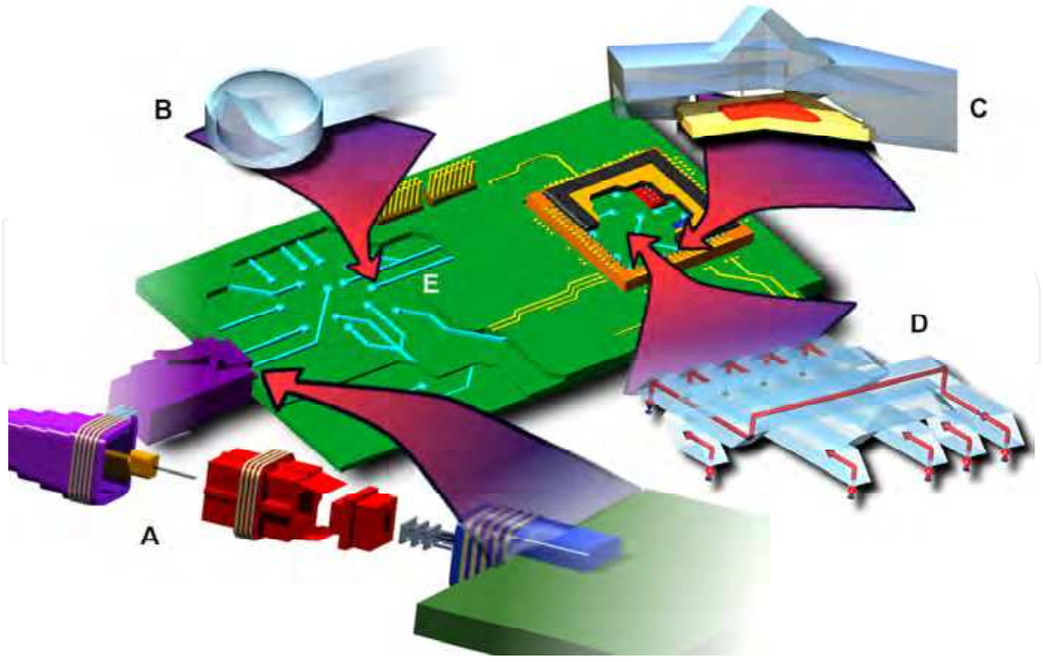


Fig. 9. Examples of micro-optical components for printed circuit board-level photonic interconnects: peripheral fiber connectors (A), out-of-plane coupling components (B), free-space intra-chip interconnection modules (C), optical redistribution layers (D) and board-integrated optical waveguides (E).

### 3.1 High-precision fiber connector components

High-precision two dimensional fiber alignment modules can offer large benefits for high-density photonic interconnects at the board-to-board and at the chip-to-chip level, where parallel light signals have to be transferred between integrated dense 2D emitter and detector arrays. Even for the telecommunication infrastructure, the availability of highly accurate, low cost, field installable two dimensional fiber connectors would boost the further integration of fiber-optics in fiber-to-the-home networks (Kim et al., 2003). Using DPW, we prototyped a 2D connector for single-mode (SM) fibers, featuring conically shaped micro-holes to ease the insertion of fibers from the backside of the fiber connector into sub-micrometer precision holes (Van Erps et al., 2006a). The conical shape of the holes, as shown in the left part of Fig. 10, has been obtained by taking advantage of the ion-ion scattering effect of protons, as explained in section 2.1. This effect becomes pronounced for proton fluences in excess of $10^7 / \mu m^2$. The optimized micro-holes for fiber-insertion feature a front side diameter of 134-$\mu m$, an inner diameter snap-fitting a fiber with cladding diameter of 125-$\mu m$, and a back side diameter of 165-$\mu m$. The connector plate features a $4 \times 8$ array of holes with a pitch of 250-$\mu m$, as shown in the left part of Fig. 11, fully compatible with the MPO fiber connector standard. Using the DPW technology we are capable of integrating alignment holes into the design during one single irradiation step. The fabricated alignment holes are two holes with a diameter of 700-$\mu m$, compatible with standard mechanically transferable (MT)-ferrule metal guide pins. By measuring the rim of the micro-holes with an optical profiler we find a standard deviation on the hole positions below 0.8-$\mu m$ (limited by the measurement apparatus). We measured an average in-line coupling loss over the complete 2D array of only 0.06-$dB$ in the telecom C and

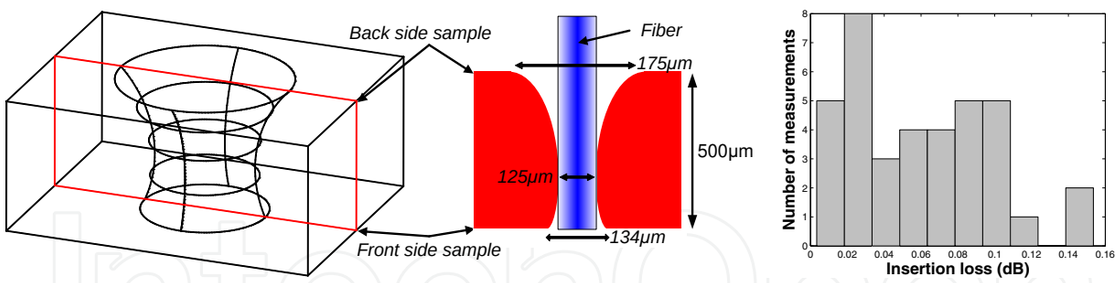


Fig. 10. Left: schematic representation of the conical profile of the micro-holes allowing an easy fiber insertion from the back side (not drawn to scale). Right: histogram of in-line fiber-to-fiber coupling efficiencies.

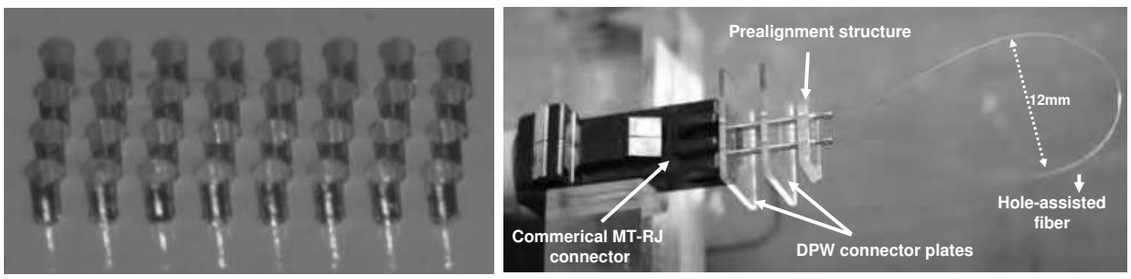


Fig. 11. Left: array of micro-holes fabricated through DPW. Right: experimental setup for coupling efficiency measurements of the assembled 180°-bend socket mounted on a commercial MT-RJ connector.

L bands, with a maximum coupling loss of 0.15-$dB$ (Van Erps et al., 2006a). The histogram of the connector losses over the whole array is shown in the right-hand side of Figure 10. To populate these fiber connectors, we developed an in-situ interferometric setup which allows the monitoring of the fiber tip position during the insertion process (Van Erps et al., 2010). This ensures an accurate fiber tip position, coinciding with the fiber connector's front facet and across the fiber array in cases where post-insertion polishing is not possible. Furthermore, the quality of the fiber tip can be assessed as well using this setup.
Recently, we also introduced a novel type of small-form-factor 180°-bend SM fiber socket, which would greatly enhance the organization of distribution frames in today's optical telecom networks, by achieving a high-efficiency connection between two parallel positioned adjacent standard telecom fibers (Van Erps et al., 2008b). This connection is achieved by means of a specially designed low bending loss hole-assisted fiber (Van Erps et al., 2008c), which allows for bend radii down to 2-$mm$ without suffering from bending loss. The realized 180°-bend SM fiber socket is illustrated in the right part of Fig. 11. We achieved coupling losses as low as 0.5-$dB$ for the total link when using it on a commercial MT-RJ connector, which illustrates once more that DPW allows for the fabrication of high-precision low-loss fiber connectors.

### 3.2 Coupling structures for printed circuit board-level optical interconnections

Now, we focus our attention at short-range optical interconnects at the printed circuit board (PCB)-level. In present-day electronic systems, the speed of CMOS-based micro-processors is relentlessly increasing, leading to a long-predicted and overwhelming interconnect

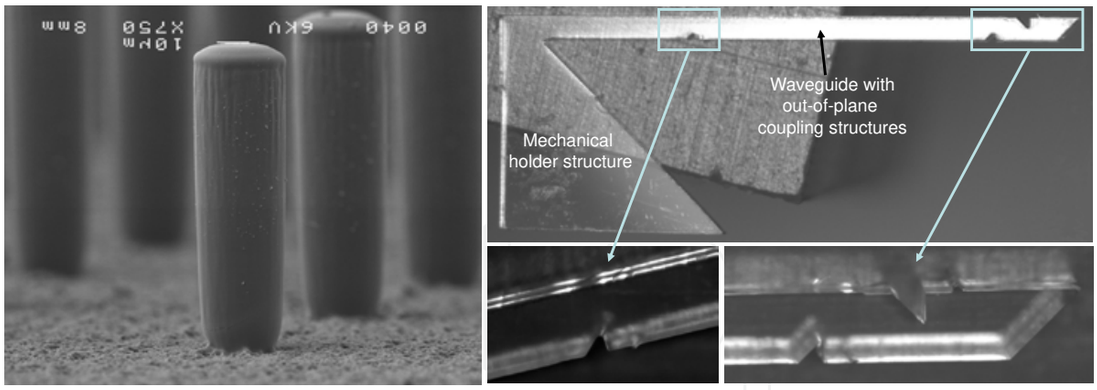


Fig. 12. Left: SEM image of DPW fabricated pillars with a diameter of 20-$\mu m$ and a height of 96-$\mu m$. Right: DPW fabricated prototype of a branching waveguide with three integrated out-of-plane coupling micro-mirrors.

bottleneck. Although it is unsure when the physical limitations of the existing copper-based electrical interconnects will be reached, it is clear that a solution needs to be provided (ITRS, 2007). A potential candidate is the introduction of parallel optical interconnections as a wire-complementing technology (Miller, 2000). This is illustrated in Fig. 9. Such an optically enhanced interconnect approach should allow to seamlessly extend the optical fiber data path to the very heart of the data-processing chips. While in recent years a large number of optical interconnect approaches have been proposed at the PCB-level, they do not yet provide a cost-effective solution, mainly due to a lack of maturity. A critical and relatively unsolved issue consists of the efficient coupling of light to and from PCB-integrated waveguides. The most commonly used approach is the use of 45° micro-mirrors, which are generally directly integrated in the PCB-embedded waveguides (Glebov et al., 2005; Hendrickx et al., 2007;a; Yoshimura et al., 1997).

To enhance the coupling efficiency when using waveguide-integrated micro-mirrors, we investigated a pillar-assisted coupling scheme, in which an optical micro-pillar is placed between a surface-mounted laser/detector and an out-of-plane coupling micro-mirror to compensate for differences in thermal expansion of the materials (Glebov et al., 2006). Our optical simulations showed that the introduction of pillars in the coupling system increases the link efficiency by several $dBs$ and that the tolerance for mechanical misalignments also strongly increases. We successfully demonstrated the fabrication of arrays of high-quality micro-pillars using DPW (Debaes et al., 2008), with an aspect ratio of almost 1:5, as shown in the scanning electron microscope (SEM) image in the left part of Fig. 12.

Another component we introduced is a light distribution component, consisting of a branching waveguide with integrated micro-mirrors (Van Erps et al., 2006). The component was designed to realize a 1-to-3 splitting of the light propagating in the waveguide, where the dimension of each integrated mirror was calculated such that it would couple out 20% of the input power. For the fabrication of the component, two different proton beam collimation apertures were used during a single irradiation for the first time. The fabricated prototype of the branching waveguide is shown in the right part of Fig. 12. The experimentally measured coupling efficiency of 21.8% for each micro-mirror is in good correspondence with the targeted value of 20%.

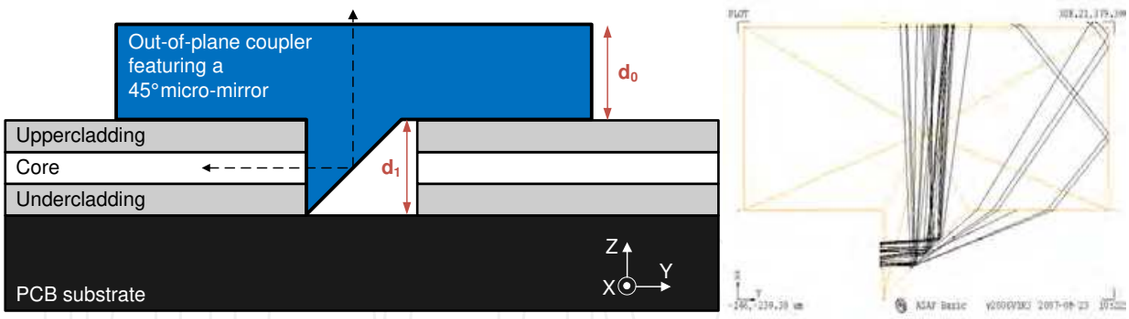


Fig. 13. Left: operation principle of a discrete out-of-plane coupler featuring a 45° micro-mirror inserted into a cavity in an optical PCB. The light propagating in the optical waveguide is coupled out-of-plane by means of a 90° deflection on the micro-mirror, or vice versa, as illustrated by the dashed arrow. Right: non-sequential ray tracing through the coupler.

As a versatile alternative to the common approach of using 45° micro-mirrors directly integrated into the waveguides, we introduced discrete out-of-plane coupling structures (Van Erps et al., 2007). We started with an out-of-plane coupling component comprising a 45° Total Internal Reflection (TIR) micro-mirror which can be readily inserted in micro-cavities formed in the PCB-integrated waveguides, as illustrated in Fig. 13. A non-sequential ray tracing through this component (also shown in Fig. 13) shows that, due to the relatively high numerical aperture of the board-embedded waveguides, quite a lot of rays are lost at the polymer-air mirror interface because they do not satisfy the condition for TIR (Van Erps et al., 2010a). Demonstrator measurements on a DPW fabricated prototype, shown in the left part of Fig. 14, showed achievable coupling losses of 0.77-$dB$ in a fiber-to-fiber scheme and a total link loss of 5.67-$dB$ when the coupler was inserted in a cavity on an optical PCB. The experimentally measured detector alignment tolerances were in excellent agreement with optical simulations (Van Erps et al., 2010a).
The coupling efficiency can be strongly increased by integrating cylindrical micro-lenses in the coupler and by introducing a curvature in the micro-mirror to ensure total internal reflection at the micro-mirror as well as beam collimation at the same time (Van Erps et al., 2008d). The optimal design (i.e. the curvature of the cylindrical lens and of the micro-mirror) was determined by coupling numerical optimization algorithms to optical design tools in an iterative process, to maximize the efficiency of the optical system with free-form surfaces described by means of Bézier polynomials. As shown in Table 1, an improvement of 1-$dB$ in comparison to the 'standard' 45° mirror coupler was measured experimentally for the enhanced coupler shown in the right part of Fig. 14. Another way to improve the achievable coupling efficiency is to apply a metal reflection coating on the micro-mirror. We experimentally demonstrated this with a fully embedded micro-mirror insert, where a mirror loss of only 0.35-$dB$ was achieved (Hendrickx et al., 2008). A second important advantage of using a coated micro-mirror is that it avoids problems that could be caused by the penetration of adhesives in the optical via during the mounting phase of the out-of-plane coupler. Furthermore, there is a risk of dust contamination or moisture adsorption in the cavity, which would severely impair the TIR operation of the mirror. When a metallized mirror is used instead, the entire cavity which accommodates the out-of-plane coupler can

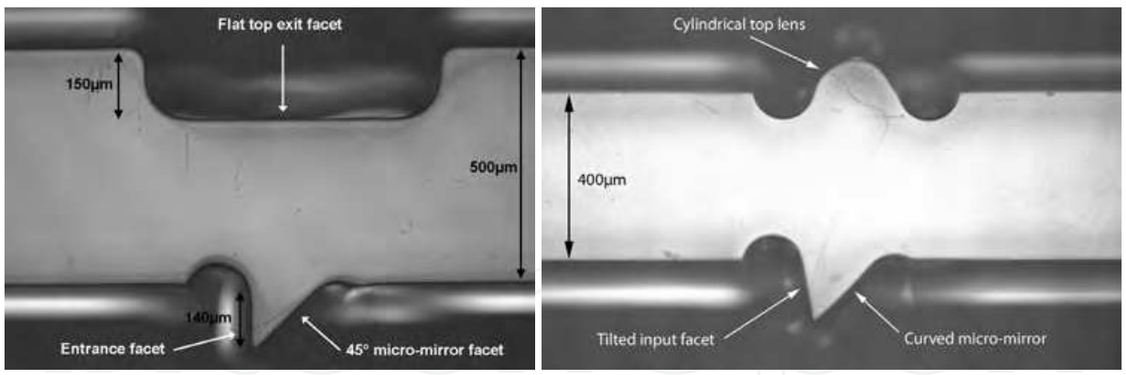


Fig. 14. Fabricated out-of-plane coupler using DPW (left) and its enhanced version featuring a curved micro-mirror and an integrated cylindrical micro-lens (right).

Table 1. Out-of-plane coupling efficiency measurement results for a coupler with a standard 45° micro-mirror, and for an enhanced coupler with curved micro-mirror and integrated cylindrical lens at the top facet.

| Component | Fiber-to-fiber | On PCB demonstrator |
|---|---|---|
| **Standard coupler** | 83.7% (-0.77-$dB$) | 27.1% (-5.67-$dB$) |
| **Enhanced coupler** | 80.0% (-0.97-$dB$) | 33.9% (-4.70-$dB$) |

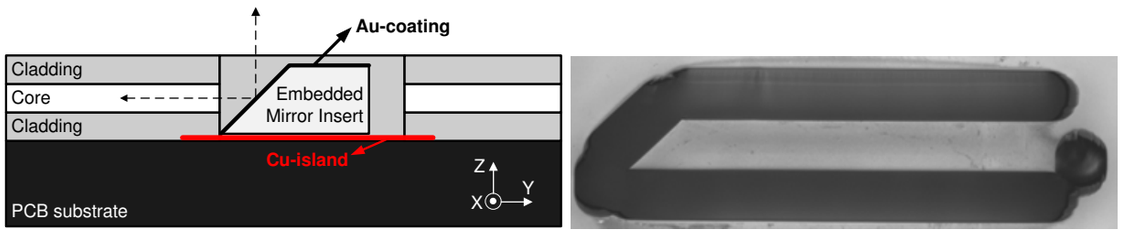


Fig. 15. Left: operation principle of an embedded mirror insert integrated into a cavity in a PCB. Right: fabricated DPW micro-mirror insert, after the chemical etching step.

be filled with adhesive to avoid the presence of undesired air gaps in the optical PCB, as illustrated in Fig. 15.

The interest in multilayer optical interconnections on the PCB-level has grown recently in view of their potential for higher integration densities and more flexible routing schemes (Hwang et al., 2007). Moreover, they can take full advantage of the 2D characteristics of 2D optoelectronic devices such as Vertical Cavity Surface Emitting Laser (VCSEL) and photodetector arrays. To this end, we present in Fig. 16 the first prototypes of multilayer out-of-plane coupling components (Van Erps et al., 2007). Finally, we introduced intra-layer coupling components, allowing to couple light from one waveguide layer to another when used on multilayer optical boards (Van Erps et al., 2007a). These intra-plane coupling components are shown in Fig. 17. Besides the enhanced functionality and increased flexibility, the biggest advantage of discrete coupling components over waveguide-integrated coupling structures, which have to be compatible with standard high-temperature PCB manufacturing processes, is that discrete couplers can be inserted at a very late stage of the PCB fabrication process.

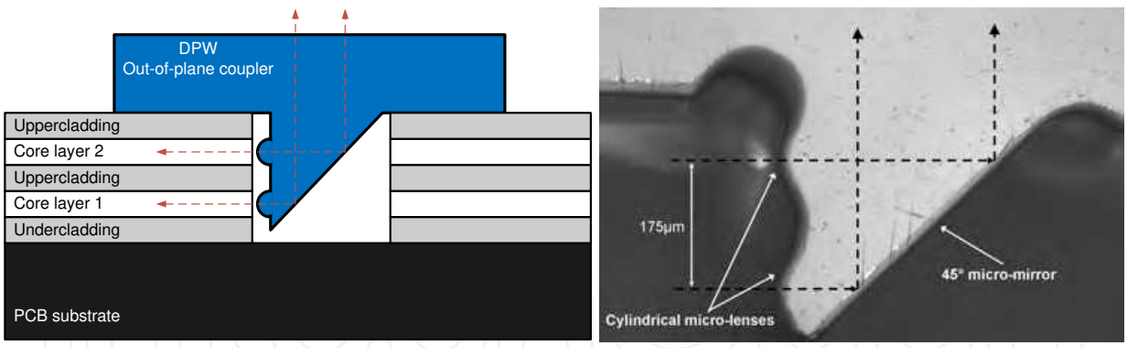


Fig. 16. Left: operation principle of a discrete two-layer out-of-plane coupler featuring a 45° micro-mirror and integrated cylindrical micro-lenses. The light paths are indicated by the dashed arrows. Right: first prototype of a DPW multilayer out-of-plane coupler with monolithically integrated cylindrical micro-lenses at the input facet.

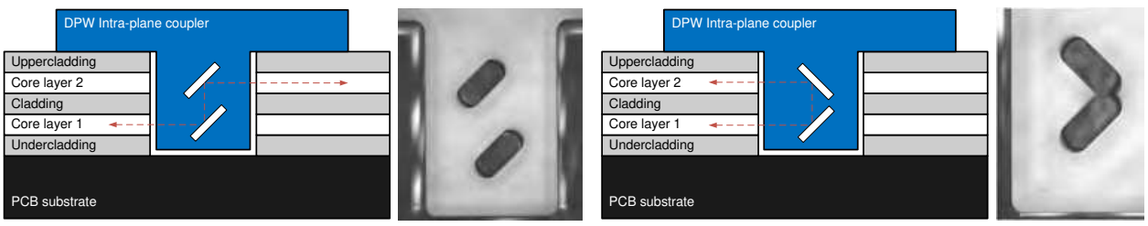


Fig. 17. Schematic working principle and fabricated inter-plane coupling components with preservation of propagation direction (left) and with inversion of propagation direction (right). The light path is indicated by the dashed arrow.

### 3.3 Intra-chip optical interconnect modules

Whereas discrete out-of-plane-couplers can be fabricated with only a single irradiation and etching step, other more complex interconnection components require a more intricate combination of high-quality optical surfaces, spherical micro-lenses and micro-mechanical alignment features. An example of such a component is the prism-based intra-MCM interconnect module shown in Fig. 18. Our approach here is based on a micro-prism reflector which transports and routes data-carrying light beams from a micro-emitter array to a micro-detector array, hence bridging intra-chip interconnection lengths ranging between a few tens of millimeters down to only a few millimeters. On its way from source to detector, each of the multiple beams are collimated, reflected at the 45° angled facets and refocussed by micro-lenses. We have shown that this type of interconnect module has the potential to provide the highly desirable massive parallel high-speed interconnects needed for future generation intra-MCM level interconnections (Debaes et al., 2003). We have been working towards a massively parallel intra-chip interconnect demonstrator that has a channel density above 4000 channels/$cm^2$ and hence provides us with low-cost, chip compatible, plug-and-play, commercially viable interconnect solutions. We were not only looking at the fabrication of the module, but we have also investigated how the component can be reliably attached above a dense optoelectronic chip (Vervaeke et al., 2006). We have therefore developed a solution consisting of a spacer plate surrounding and accurately positioning the optoelectronic chip. The spacer plate and the optical interconnection module were attached to each other via precise steel micro-spheres, and a detailed Monte-Carlo tolerance analysis regarding fabrication and assembly was performed (Vervaeke et al., 2006).

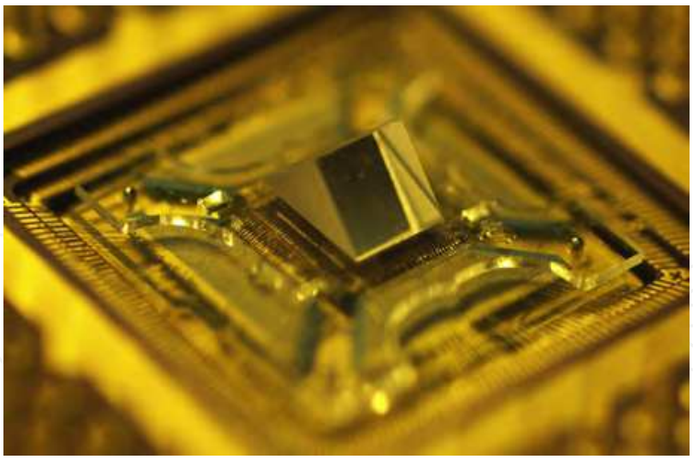

Fig. 18. Our free-space intra-MCM interconnection module mounted on top of a dense optoelectronic chip by means of a DPW high-precision spacer structure.

## 4. Micro-optical detection modules for absorbance and fluorescence measurements

In this section, we describe DPW components that were designed and fabricated for absorbance and fluorescence detection. To determine the result of a biochemical analysis, molecules have to be detected and quantified. Over the last few decades, various micro total analysis systems ($\mu$TAS) –also called lab-on-a-chip, miniaturized, or micro-fluidic analysis systems– have been developed, which integrate different chemical processes (sample pre-treatment, mixing, chromatographic, or electrophoresis separation) on a single chip (Manz et al., 1990; Monat et al., 2007). In these systems, a good molecule detection is one of the biggest challenges. To this end, optical techniques are often used, to measure the absorbance or fluorescence of molecules. Fluorescence measurements are very sensitive and selective, but in general an extra sample preparation step is required to label the often non-fluorescent molecules with a fluorescent dye. Absorbance measurements are less sensitive but don't need this extra labelling step. Up to now, only classical microscopes are sufficiently sensitive to detect small amounts of molecules in the nanoliter detection volumes on the chip. These instruments are, unfortunately, too big and too expensive for integration in portable devices. Therefore, there is a large demand for efficient, small and robust optical detection units. Recently, we developed this kind of detection systems based on plastic micro-optical components and optical fibers, targeting a strong integration of the micro-optics around the micro-fluidic channels as well as a high sensitivity at low cost. The proof-of-concept was demonstrated for two systems, optimized for fluorescence and absorbance detection in a specific type of micro-fluidic channel.

In a first system, a plastic micro-optical light coupler was used for the detection of the absorbance of molecules in a silicon micro-fluidic chip (Van Overmeire et al., 2008). Its concept is shown in the left part of Fig. 19. By means of light reflections on the aluminum-coated curved sidewalls of the coupler and on the sidewalls of the channel, the excitation light was coupled in and out of the micro-fluidic channel in order to excite the molecules and measure their absorbance. In this configuration, a long optical path length of 1.5-$mm$ is realized in which the light can interact with the molecules present in the channel, allowing

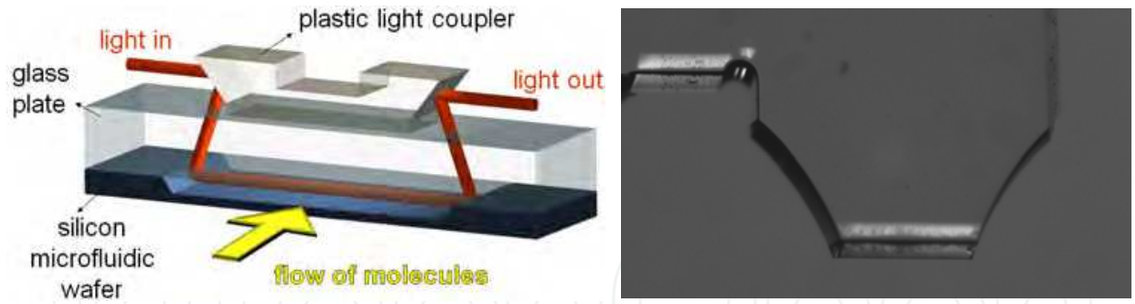


Fig. 19. Plastic light coupler for absorbance detection in silicon micro-fluidic devices: schematic (left) and DPW-fabricated prototype of the coupler before the application of a metal reflection coating (right).

the detection of low molecule concentrations. Since the micro-optical detection unit can be separated from the micro-fluidic chip, several of these units can be combined to perform parallel measurements at different locations on the chip, which makes this plastic light coupler a flexible detection tool that can be used on different types of chips. A prototype of the plastic micro-optical coupler, fabricated with DPW, is shown in the right part of Fig. 19. The smallest molar concentration of a coumarin dye sample measured experimentally with this system was 4.2-$\mu M$ (i.e. the detection limit for a signal-to-noise ratio of 3.3). Currently we are optimizing the setup to decrease this value and to reach a submicromolar detection limit.

In the second system, molecules were excited by means of refractive micro-lenses and they were detected in standard silica capillaries used in e.g. chromatographic applications. The concept is shown in Fig. 20 (Van Overmeire et al., 2008a). The micro-lenses were monolithically integrated around the capillary micro-channel and are therefore automatically aligned, eliminating the need for active alignment. The optical path length was determined by the inner diameter of the capillary (typically in the range of 20-$\mu m$ to 150-$\mu m$) and hence the sensitivity of the absorbance detection of this system was lower than in the previous system. However, the main goal of this plastic detection unit was to enable the measurement of a wide variety of molecule concentrations. Indeed, in this setup, absorbance measurements of relatively high concentrations of molecules were combined with fluorescence measurements of extremely low concentrations of molecules, which of course had to be labeled with a fluorescent dye prior to the detection. The detection system was designed by means of non-sequential ray tracing simulations and prototyped using DPW. The prototype of this system is shown in the right part of Fig. 20. The experimentally achieved detection limit (for a signal-to-noise ratio of 3.3) for the detection of various molar concentrations of coumarin dyes, measured 1.7-$pM$ for fluorescence analysis and 0.34-$\mu M$ for absorbance measurements in capillaries with an inner diameter of 150-$\mu m$ (Van Overmeire et al., 2008a).

Our first steps towards integrated micro-optical detection systems have been succesful and we are now working on testing these two systems in a variety of practical applications, such as the detection of chromatographic separations and the characterization of lubricant oils in industrial machines (Van Overmeire et al., 2010). This allows for the optimization of the robustness and reproducibility of the systems, which will pave the way towards clinical diagnostic lab-on-a-chip devices, which will undoubtedly feature in every doctor's office for point-of-care analysis.

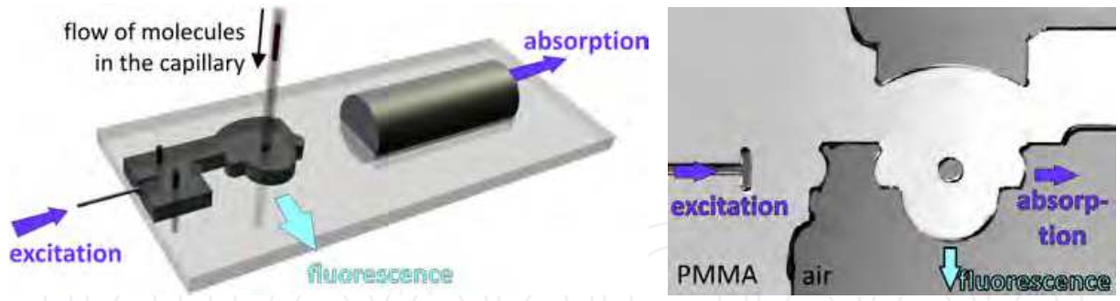


Fig. 20. Miniaturized detection system for fluorescence and absorbance measurements: schematic (left) and DPW-fabricated detection system (right).

## 5. Conclusion

We presented deep proton writing as a versatile, generic rapid prototyping technology, which enables the fabrication of a wide variety of micro-optical and micro-mechanical components. We showed that DPW is a viable technology for fabricating prototypes of deep micro-optical structures with high aspect ratio. The basic process of DPW consists of an irradiation of selected areas with swift protons. Two chemical process steps can then be applied to the irradiated sample to either develop the high proton fluence areas by a selective etching solvent and/or to create a swelling of the circular footprint of the lower fluence areas into hemispherical micro-lenses. Through a series of optimizations for the irradiation setup, as well as the etching and the swelling processes, we are capable of making high-grade prototype micro-optical and micro-mechanical elements.

To illustrate the potential of the DPW process, we gave an overview of the micro-components which were prototyped in recent years, targeting applications in optical interconnects and bio-photonics, including high-precision fiber connectors, out-of-plane coupling structures featuring high-quality micro-mirrors, and fluorescence and absorption detection modules. While DPW is clearly a prototyping technology, we have also shown that one of its important assets is that it is compatible with low-cost mass fabrication through the formation of a mould from the DPW master. This mould can then be used in a final micro-injection moulding or hot embossing step, allowing high-volume replication in various high-tech plastics.

## 6. Acknowledgments

This work was supported in part by BELSPO-IAP, FWO, GOA, IWT-SBO, the European Network of Excellence on Micro-Optics NEMO, the European Network of Excellence on Biophotonics Photonics4Life, the Hercules and Methusalem foundations, and by the OZR of the Vrije Universiteit Brussel. The work of J. Van Erps, C. Debaes and H. Ottevaere, was supported by the FWO (Fund for Scientific Research - Flanders) under a post-doctoral research fellowship.

## 7. References

Acharya, B.R.; Ramachandran, S.; Krupenkine, T.; Huang, C.C. & Rogers, J.A. (2003). Tunable optical fiber devices based on broadband long period gratings and pumped microfluidics. *Applied Physics Letters*, Vol. 83, pp. 4912-4914.

Becker, E.W.; Erfield, W.; Hagmann, P.; Maner, A. & Munchmeyer, D. (1986). Fabrication of microstructures with high aspect ratios and great structural heights by synchrotron radiation lithography, galvanoforming, and plastic moulding (LIGA process). *Microelectronics Engineering*, Vol. 4, pp. 35-56.

Bethe, H.A. (1930). Zur Theorie des Durchgangs schneller Korpuskularstrahlen durch Materie. *Annalen der Physik*, Vol. 397, No. 3, pp. 325-400.

Bohr, N. (1913). On the Constitution of Atoms and Molecules, Part I. *Philosophical Magazine*, Vol. 26, pp. 1–24.

Bohr, N. (1948). *Matematisk-Fysiske Meddelelser af Det Kongelige Danske Videnskabernes Selskab*, Vol. 18, No. 8, pp. 144.

Davies, M.A.; Evans, C.J.; Patterson, S.R.; Vohra, R. & Bergner, B. (2003). Application of precision diamond machining to the manufacture of micro-photonics components. *Proceedings of the SPIE*, Vol. 5183, pp. 94-108.

Debaes, C.; Vervaeke, M.; Baukens, V.; Ottevaere, H.; Vynck, P.; Tuteleers, P.; Volckaerts, B.; Meeus, W.; Brunfaut, M.; Van Campenhout, J.; Hermanne, A.; Thienpont, H. (2003). Low-cost microoptical modules for MCM level optical interconnections. *IEEE Journal of Selected Topics in Quantum Electronics*, Vol. 9, No. 2, pp. 518-530.

Debaes, C.; Vervaeke, M.; Volckaerts, B.; Van Erps, J.; Desmet, L.; Ottevaere, H.; Vynck, P.; Gomez, V.; Hermanne, A. & Thienpont, H. (2005). Low-cost micro-optical modules for board level optical interconnections. *IEEE LEOS Newsletter*, Vol. 19, pp. 12-14.

Debaes, C.; Van Erps, J.; Vervaeke, M.; Volckaerts, B.; Ottevaere, H.; Gomez, V.; Vynck, P.; Desmet, L.; Krajewski, R.; Ishii, Y.; Hermanne, A. & Thienpont, H. (2006). Deep Proton Writing: a rapid protoyping polymer microfabrication tool for micro-optical modules. *New Journal of Physics*, Vol. 8, 270.

Debaes, C.; Van Erps, J.; Karppinen, M.; Hiltunen, J.; Suyal, H.; Last, A.; Lee, M.G.; Karioja, P.; Taghizadeh, M.; Mohr, J.; Thienpont, H. & Glebov, A.L. (2008). Fabrication method to create high-aspect ratio pillars for photonic coupling of board level interconnects. *Proceedings of the SPIE*, Vol. 6992, 69920T.

Desmet, L.; Van Overmeire, S.; Van Erps, J.; Ottevaere, H.; Debaes, C. & Thienpont, H. (2007). Fabrication of an array of concave refractive microlenses using elastomeric inverse moulding and vacuum casting. *Journal of Micromechanics & Microengineering*, Vol. 17, No. 1, pp. 81-88.

Ehrfeld, W. & Schmidt, A. (1998). Recent developments in deep X-ray lithography. *Journal of Vacuum Science & Technology B*, Vol. 16, pp. 3526-3534.

Fano, U. (1963). Penetration of protons, alpha particles and mesons. *Annual Review of Nuclear Science*, Vol. 13, pp. 1.

Glebov, A.; Roman, J.; Lee, M.G. & Yokouchi, K. (2005). Optical interconnect modules with fully intgrated reflector mirrors. *IEEE Photonics Technology Letters*, Vol. 17, No. 7, pp. 1540-1542.

Glebov, A.L.; Bhusari, D.; Kohl, P.; Bakir, M.S.; Meindl, J.D. & Lee, M.G. (2006). Flexible pillars for displacement compensation in optical chip assembly. *IEEE Photonics Technology Letters*, Vol. 18, No. 8, pp. 974-976.

Gomez, V.; Ottevaere, H.; Thienpont, H. (2008). Mach-Zehnder interferometer for real-time in situ monitoring of refractive microlens characteristics at the fabrication level. *IEEE Photonics Technology Letters*, Vol. 20, No. 9, pp. 748-750.

Heckele, M. & Schomburg, W.K. (2004). Review on micro molding of thermoplastic polymers. *Journal of Micromechanics & Microengineering*, Vol. 14, pp. R1-R14.

Hendrickx, N.; Van Erps, J.; Van Steenberge, G.; Thienpont, H. & Van Daele, P. (2007). Laser ablated micromirrors for Printed Circuit Board integrated optical interconnections. *IEEE Photonics Technology Letters*, Vol. 19, No. 11, pp. 822-824.

Hendrickx, N.; Van Erps, J.; Van Steenberge, G.; Thienpont, H.; Van Daele, P. (2007a). Tolerance analysis for multilayer optical interconnections integrated on a Printed Circuit Board. *Journal of Lightwave Technology*, Vol. 25, No. 9, pp. 2395-2401.

Hendrickx, N.; Van Erps, J.; Bosman, E.; Debaes, C.; Thienpont, H. & Van Daele, P. (2008). Embedded micromirror inserts for optical printed circuit boards. *IEEE Photonics Technology Letters*, Vol. 20, No. 20, pp. 1727-1729.

Hwang, S.H.; Cho, M.H.; Kang, S.-K.; Lee, T.-W.; Park, H.-H. & Rho, B.S. (2007). Two-dimensional optical interconnection based on two-layered optical printed circuit board. *IEEE Photonics Technology Letters*, Vol. 17, No. 6, pp. 411-413.

International Technology Roadmap for Semiconductors [Online] Available: http://www.itrs.net/reports.html

Kim, J.; Nuzman, C.J.; Kumar, B.; Lieuwen, D.F.; Kraus, J.S.; Weiss, A.; Lichtenwalner, C.P.; Papazian, A.R.; Frahm, R.E.; Basavanhally, N.R.; Ramsey, D.A.; Aksyuk, V.A.; Pardo, F.; Simon, M.E.; Lifton, V.; Chan, H.B.; Haueis, M.; Gasparyan, A.; Shea, H.R.; Arney, S.; Bolle, C.A.; Kolodner, P.R.; Ryf, R.; Neilson, D.T.; Gates, J.V. (2003). 1100 x 1100 port MEMS-based optical crossconnect with 4-dB maximum loss. *IEEE Photonics Technology Letters*, Vol. 15, No. 11, pp. 1537-1539.

Kumakhov, M.A. & Komarov, F.F. (1981). *Energy Loss and Ion Ranges in Solids*, Gordon and Breach, London.

Lee, E.H.; Rao, G.R.; Mansur, L.K. (1999). LET effect on cross-linking and scission mechanisms of PMMA during irradiation . *Radiation Physics and Chemistry*, Vol. 55, No. 3, pp. 293–305.

Love, J.C.; Anderson, J.R. & Whitesides, G.M. (2001). Fabrication of three-dimensional microfluidic systems by soft lithography. *MRS Bulletin*, Vol. 26, No. 7, pp. 523-528.

Manz, A.; Graber, N. & Widmer, H.M. (1990). Miniaturized total chemical analysis systems: A novel concept for chemical sensing. *Sensors & Actuators B, Chemistry*, Vol. 1, pp. 244-248.

McClure, E. (1991). Manufacturers turn precision optics with diamond. *Laser Focus World*, Vol. 2, pp. 95-105.

Mihailov, S. & Lazare, S. (1993). Fabrication of refractive microlens arrays by excimer laser ablation of amorphous teflon. *Applied Optics*, Vol. 32, pp. 6211-6218.

Miller, D.A.B. (2000). Rationale and challenges for optical interconnects to electronic chips. *Proceedings of the IEEE*, Vol. 88, No. 6, pp. 728-749.

Monat, C.; Domachuk, P.; Eggleton, B.J. (2007). Integrated optofluidics: A new river of light. *Nature Photonics*, Vol. 1, No. 2, pp. 106-114.

Ottevaere, H.; Volckaerts, B.; Lamprecht, J.; Schwider, J.; Hermanne, A.; Veretennicoff, I.; Thienpont, H. (2002). Two-dimensional plastic microlens arrays by deep lithography with protons: fabrication and characterization. *Journal of Optics A: Pure and Applied Optics*, Vol. 4, No. 4, pp. S22-S28.

Ottevaere, H.; Cox, R.; Herzig, H.P.; Miyashita, T.; Naessens, K.; Taghizadeh, M.; Volkel, R.; Woo, H.J.; Thienpont, H. (2006). Comparing glass and plastic refractive microlenses

fabricated with different technologies. *Journal of Optics A: Pure and Applied Optics*, Vol. 8, No. 7, pp. S407-S429.

Papanu, J.S.; Soane, D.S.; Bell, A.T.; Hess, D.W. (1989). Transport models for swelling and dissolution of thin polymer films. *Journal of Applied Polymer Science*, Vol. 38, No. 5, pp. 859-885.

Rogers, J.A. (2001). Rubber stamping for plastic electronics and fiber optics. *MRS Bulletin*, Vol. 26, No. 7, pp. 530-534.

Thienpont, H.; Baukens, V.; Ottevaere, H.; Volckaerts, B.; Tuteleers, P.; Vynck, P.; Vervaeke, M.; Debaes, C.; Verschaffelt, G.; Hermanne, A. & Veretennicoff, I. (2001). Free-space micro-optical modules: the missing link for photonic interconnects to silicon chips. *Opto-electronics Review*, Vol. 9, pp. 238-247.

Van Erps, J.; Bogaert, L.; Volckaerts, B.; Debaes, C. & Thienpont, H. (2006). Prototyping micro-optical components with integrated out-of-plane coupling structures using deep lithography with protons. *Proceedings of the SPIE*, Vol. 6185, 618504.

Van Erps, J.; Volckaerts, B.; Van Amerongen, H.; Vynck, P.; Krajewski, R.; Debaes, C.; Watté, J.; Hermanne, A. & Thienpont, H. (2006a). High-precision 2-D SM fiber connectors fabricated through Deep Proton Writing. *IEEE Photonics Technology Letters*, Vol. 18, No. 10, pp. 1164-1166.

Van Erps, J.; Hendrickx, N.; Debaes, C.; Van Daele, P. & Thienpont, H. (2007). Discrete out-of-plane coupling components for printed circuit board-level optical interconnections *IEEE Photonics Technology Letters*, Vol. 19, No. 21, pp. 1753-1755.

Van Erps, J.; Hendrickx, N.; Debaes, C.; Van Daele, P. & H. Thienpont, H. (2007a). Pluggable inter-plane couplers for multilayer optical interconnections. *Proceedings of the 33rd European Conference on Optical Communication (ECOC'07)*, pp. 54.

Van Erps, J.; Wissmann, M.; Guttmann, M.; Hartmann, M.; Desmet, L.; Debaes, C.; Mohr, J. & Thienpont, H. (2008). Replication of deep micro-optical components prototyped by Deep Proton Writing. *Proceedings of the SPIE*, Vol. 6992, 699209.

Van Erps, J.; Wissmann, M.; Guttmann, M.; Hartmann, M.; Debaes, C.; Mohr, J. & Thienpont, H. (2008a). Hot embossing of microoptical components prototyped through Deep Proton Writing. *IEEE Photonics Technology Letters*, Vol. 20, No. 18, pp. 1539-1541.

Van Erps, J.; Debaes, C.; Singh, R.; Nasilowski, T.; Mergo, P.; Wojcik, J.; Aerts, T.; Terryn, H.; Vynck, P.; Watté, J. & Thienpont, H. (2008b). Mass Manufacturable 180°-Bend Single-Mode Fiber Socket Using Hole-Assisted Low Bending Loss Fiber. *IEEE Photonics Technology Letters*, Vol. 20, No. 3, pp. 187-189.

Van Erps, J.; Debaes, C.; Nasilowski, T.; Watté, J.; Wojcik, J. & Thienpont, H. (2008c). Design and tolerance analysis of a low bending loss hole-assisted fiber using statistical design methodology. *Optics Express*, Vol. 16, No. 7, pp. 5061-5074.

Van Erps, J.; Heyvaert, S.; Debaes, C.; Van Giel, B.; Hendrickx, N.; Van Daele, P. & Thienpont, H. (2008d). Enhanced pluggable out-of-plane coupling components for printed circuit board-level optical interconnections. *Proceedings of the SPIE*, Vol. 6992, 69920S.

Van Erps, J.; Pakula, A.; Tomczewski, S.; Salbut, L.; Vervaeke, M. & Thienpont, H. (2010). In situ interferometric monitoring of fiber insertion in fiber connector components. *IEEE Photonics Technology Letters*, Vol. 22, No. 1, pp. 60-62.

Van Erps, J.; Debaes, C. & Thienpont, H. (2010a). Design and tolerance analysis of out-of-plane coupling components for printed circuit board-level optical interconnections. *IEEE Journal of Selected Topics in Quantum Electronics*, Vol. 16, No. 5, pp. 1347-1354.

Van Overmeire, S.; Ottevaere, H.; Nieradko, L.; Marc, P.; Mappes, T.; Mohr, J.; Gorecki, C. & Thienpont, H. (2008). Plastic light coupler for absorbance detection in silicon microfluidic devices. *Proceedings of the 14th MicroOptics Conference (MOC'08)*, pp. 92-93.

Van Overmeire, S.; Ottevaere, H.; Desmet, G. & Thienpont, H. (2008a). Miniaturized detection system for fluorescence and absorbance measurements in chromatographic applications. *IEEE Journal of Selected Topics in Quantum Electronics*, Vol. 14, No. 1, pp. 140-150.

Van Overmeire, S.; Ottevaere, H.; Mignani, A.G.; Ciaccheri, L.; Desmet, G.; Thienpont, H. (2010). Tolerance analysis of a micro-optical detection system for on-line monitoring of lubricant oils. *Journal of Micromechanics and Microengineering*, Vol. 20, No. 10, 105018.

Vervaeke, M.; Debaes, C.; Volckaerts, B.; Thienpont, H. (2006). Optomechanical Monte Carlo tolerancing study of a packaged free-space intra-MCM optical interconnect system. *IEEE Journal of Selected Topics in Quantum Electronics*, Vol. 12, No. 5, pp. 988-996.

Volckaerts, B. (2004). *Deep lithography with ions*, PhD thesis, Vrije Universiteit Brussel.

Vynck, P.; Volckaerts, B.; Vervaeke, M.; Ottevaere, H.; Tuteleers, P.; Cosentino, L.; Finocchiaro, P.; Pappalardo, A.; Hermanne, A.; Thienpont, H. (2002). Beam monitoring enhances deep proton lithography: towards high-quality micro-optical components *Proceedings of the IEEE/LEOS Benelux Chapter*, pp. 298-301.

Wissmann, M.; Guttmann, M.; Mohr, J.; Hartmann, M.; Wilson, S.; Moran-Iglesias, C.-J.; Van Erps, J.; Krajewski, R.; Parriaux, O. & Tonchev, S. (2008). Replication of micro-optical components and nano-structures for mass production. *Proceedings of the SPIE*, Vol. 6992, 699208.

Yoshimura, R.; Hikita, M.; Usui, M.; Tomaru, S. & Imamura, S. (1997). Polymeric optical waveguide films with 45° mirrors formed with a 90° V-shaped diamond blade. *Electronics Letters*, Vol. 33, No. 15, pp. 1311-1312.

Zhang, X.; Jiang, X.N. & Sun, C. (1999). Micro-stereolithography of polymeric and ceramic microstructures. *Sensors Actuators*, Vol. 77, pp. 149-156.

Ziegler, J.F. (1980). *Handbook of Stopping Cross Sections for Energetic Ions in All Elements vol 5*, Pergamon, Oxford.


**Rapid Prototyping Technology - Principles and Functional Requirements**

Edited by Dr. M. Hoque

ISBN 978-953-307-970-7
Hard cover, 392 pages
**Publisher** InTech
**Published online** 26, September, 2011
**Published in print edition** September, 2011

Modern engineering often deals with customized design that requires easy, low-cost and rapid fabrication. Rapid prototyping (RP) is a popular technology that enables quick and easy fabrication of customized forms/objects directly from computer aided design (CAD) model. The needs for quick product development, decreased time to market, and highly customized and low quantity parts are driving the demand for RP technology. Today, RP technology also known as solid freeform fabrication (SFF) or desktop manufacturing (DM) or layer manufacturing (LM) is regarded as an efficient tool to bring the product concept into the product realization rapidly. Though all the RP technologies are additive they are still different from each other in the way of building layers and/or nature of building materials. This book delivers up-to-date information about RP technology focusing on the overview of the principles, functional requirements, design constraints etc. of specific technology.

**How to reference**

In order to correctly reference this scholarly work, feel free to copy and paste the following:

Jürgen Van Erps, Michael Vervaeke, Christof Debaes, Heidi Ottevaere, Alex Hermanne and Hugo Thienpont (2011). Deep Proton Writing: A Rapid Prototyping Tool for Polymer Micro-Optical and Micro-Mechanical Components, Rapid Prototyping Technology - Principles and Functional Requirements, Dr. M. Hoque (Ed.), ISBN: 978-953-307-970-7, InTech, Available from: http://www.intechopen.com/books/rapid-prototyping-technology-principles-and-functional-requirements/deep-proton-writing-a-rapid-prototyping-tool-for-polymer-micro-optical-and-micro-mechanical-componen

INTECH
open science | open minds

**InTech Europe**
University Campus STeP Ri
Slavka Krautzeka 83/A
51000 Rijeka, Croatia
Phone: +385 (51) 770 447
Fax: +385 (51) 686 166
www.intechopen.com

**InTech China**
Unit 405, Office Block, Hotel Equatorial Shanghai
No.65, Yan An Road (West), Shanghai, 200040, China
中国上海市延安西路65号上海国际贵都大饭店办公楼405单元
Phone: +86-21-62489820
Fax: +86-21-62489821

IntechOpen